Polymer(Korea), Vol. 42, No. 5, pp. 834-840 (2018)
https://doi.org/10.7317/pk.2018.42.5.834

ISSN 0379-153X(Print)
ISSN 2234-8077(Online)

정전류 증착 방법에 의한 폴리아닐린 성장 과정에서 모폴로지 변화

김은옥† · 이재익
수원대학교 자연과학대학 화학과
(2018년 4월 6일 접수, 2018년 4월 23일 수정, 2018년 4월 26일 채택)

Morphological Changes in the Growth Process of Polyaniline During Galvanostatic Depositon

Eunok Kim† and Jaeik Lee
Department of chemistry, The University of Suwon, Hwaseoung-si, Gyeonggi-do 03601, Korea
(Received April 6, 2018; Revised April 23, 2018; Accepted April 26, 2018)

초록: 정전류 증착 방법에 의한 폴리아닐린 성장 과정에서 모폴로지 변화를 확인하였다. Chronopotentiometry 곡선에서 서로 다른 성장 과정과 관련된 세 가지 영역을 확인하였다. 초기에는, 핵 생성과 ITO 표면에서의 초기 중합 후 2-D 수평 성장이 주도적이었고, 1-D 수직 성장도 동시에 일어났다. 그 다음에, 첫 번째 층 위에서 1-D 수직 성장이 지배적으로 일어나서 섬유상 구조가 확장되었고, 결과적으로 전하 캐리어 이동도가 향상되었다. 마지막에는, 1-D 수직 성장만 일어났으므로 섬유상 구조의 상호 연결된 네트워크를 형성하였다. 중합과 분해 과정간의 경쟁에도 불구하고, 고정 전위에 도달한 후에도 고분자 성장이 진행되었으며, 약간의 응집체가 포함된 섬유상 구조가 생성되었다. 응집체에 의한 구조적 무질서는 전하 캐리어 이동도를 감소시켰으며, 이는 낮은 전도성과 높은 면저항에 밀접한 관련이 있었다.

Abstract: We have investigated morphological changes in the galvanostatic deposition of polyaniline. From the chronopotentiometric curve, we have identified three distinct regions related to the different growth process. At first, after the nucleation process and initial polymerization on the bare ITO surface, 2-D horizontal growth occurs predominantly and 1-D vertical growth occurs at the same time. And then, the dominant 1-D vertical growth process on the first layer extends the fibrous structure, which provides significantly improved charge carrier mobility. Finally, there is an only 1-D vertical growth process, resulting in an interconnected network of a fibrous structure. After reaching a stationary potential for the remaining deposition time, further growth produces a fibrous structure with some aggregate, despite the competition between the polymerization and degradation process. The aggregation-induced structural disorder reduces the charge carrier mobility, which is closely related to poor conductivity/high sheet resistance.

Keywords: polyaniline, galvanostatic, electrodeposition, morphology, growth process.

Introduction

Conducting polymers (CPs) are polymeric materials that display high electrical conductivity, good electrochemical activity, unique optical properties, and biocompatibility.[1] The greatest advantage of CPs is that their chemical, electrical, and physical properties can be tailored to the specific needs of a given application.[2] CPs can be polymerized by both chemical and electrochemical methods. Chemical methods are suitable when bulk quantities of the polymers are necessary, and these methods have so far been dominantly applied for commercial applications. Nevertheless, the most widely used technique for applications such as polymer-based electronics and electrochemical devices is electrochemical anodic oxidation. Electrochemical procedures have several advantages; they avoid usage of oxidants since CPs are obtained at the anode upon application of the positive potential, leading to increased purity. Also, because the polymer is deposited on the electrode, further electrochemical characterization is facilitated. In addition, electrochemical methods are faster than chemical methods for the polymerization of CPs (a few minutes versus a few hours).[1,3] Polyaniline (PAni) is unique among CPs because of

†To whom correspondence should be addressed.
eokim@suwon.ac.kr, ORCID 0000-0003-0344-0872

its simple non-redox doping/dedoping chemistry based on acid/base reactions. PAni is known as a mixed oxidation state polymer composed of reduced benzenoid (amine N) units and oxidized quinoid (imine N) units. It exists mainly in three well-defined oxidation states; namely, the fully reduced (leucoemeraldine), the half oxidized (emeraldine), and the fully oxidized (pernigraniline) states, with a virtually infinite number of possible oxidation states existing in between these.[4,5] Protonation of the polymer, also known as doping, is the process by which PAni becomes electrically conductive. Insulating emeraldine base (EB) can be protonated to give an emeraldine salt (ES), also called the radical cation (EB + HCl → $ES^+ + Cl^-$), and the polymer formed by radical cations and incorporated counterions can present a metallic character.[5,6] Since the electrochemical properties depend on the polymer morphology, it is of interest to observe the morphological changes related to the growth process of CPs in the electrodeposition.[4,7-9] However, there have been only few systematic studies on the galvanostatic deposition of PAni.[10] In our previous study, the morphological changes related to the growth process of PAni was visualized in both two-dimensional (2-D) and three-dimensional (3-D) images in the potentiostatic deposition.[11] Because current control is simple and can cause the reaction to proceed at a constant rate, the galvanostatic technique allows control of the film thickness by adjusting the deposition time (*t*). In this study, morphological changes related to the growth process of PAni in the galvanostatic deposition and their electrochemical properties were investigated based on the results from the chronopotentiometric (CP) curve, Fourier transform infrared (FTIR) and ultraviolet-visible (UV-Vis) absorption spectroscopy, scanning electron microscopy (SEM), and four-point probe electrical measurements.

Experimental

Galvanostatic Polymerization. Aniline (≥99.0%, Duksan Pure Chemicals) was distilled before use, and the rest of the reagents, DMSO (≥99.0%, Sigma-Aldrich) and HCl (37.0%, Duksan Pure Chemicals), were used without further purification. 0.3 M aniline was added to the 1.5 M HCl electrolyte. The deposition area of the working electrode, indium tin oxide (ITO, 9.55 ohm/sq.), was 0.25 cm^2. Pt plate (1.0 cm×1.5 cm) and Ag/AgCl (3 M NaCl) were used as the counter and reference electrode, respectively. The polymerization of aniline was performed at a current density of 1.7 mA/cm^2 using a WBCS 3000 battery cycler (WonATech). PAni in its ES form (PAni-ES) with a deposition time of 6000 s was dedoped with 0.1 M NaOH for obtaining the EB form of PAni (PAni-EB).

Characterization: FTIR spectra was recorded on an FTIR/ATR 4100 Spectrometer (Jasco) in the attenuated total reflection mode for wavenumbers of 600~2000 cm^{-1}. UV-Vis spectra was recorded on an S-3100 Spectrophotometer (Scinco) over the wavelengths of 290~1000 nm using DMSO as the solvent. High-resolution scanning electron microscopy (SEM) imaging was performed using a LYRA 3 and MAIA 3 (Tescan) system. The thickness of the films was measured using a micrometer caliper. The sheet resistance and electrical conductivity of films were measured using four-point probe with collinear probes of 0.5 cm spacing, and tested using a 2401 Source Measurement Unit (Keithley). The films with eight different deposition times: 50, 100, 300, 690, 900, 3000, 4800 and 6000 s, which are denoted for simplicity as 50s, 100s, 300s, 690s, 900s, 3000s, 4800s, and 6000s, respectively. In the case of the 50s and 100s, FTIR and UV-Vis. spectroscopy cannot be performed because the amount of sample required for the measurement is insufficient.

Results and Discussion

The CP (voltage-time transient) curve obtained during the deposition of PAni is given in Figure 1. The optimum current density was determined to be 1.7 mA/cm^2 based on our previous work, which was performed at various current densities (1.4, 1.6, 1.7, 2.0, and 2.3 mA/cm^2).[12] The curve shows three distinct regions related to the different growth processes: region 1 (R-1), region 2 (R-2), and region 3 (R-3). In the inset of Figure 1, the CP curve for the first 350 s is presented. It is generally accepted that the first step in the electrochemical polymerization of aniline is the formation of the primary radical

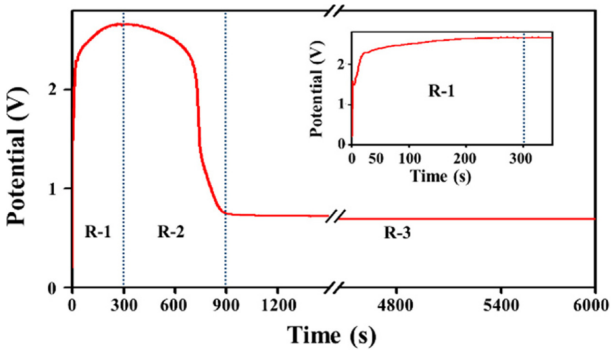

Figure 1. Chronopotentiometric curve obtained during the deposition of PAni. Inset: Magnified curve of region 1.

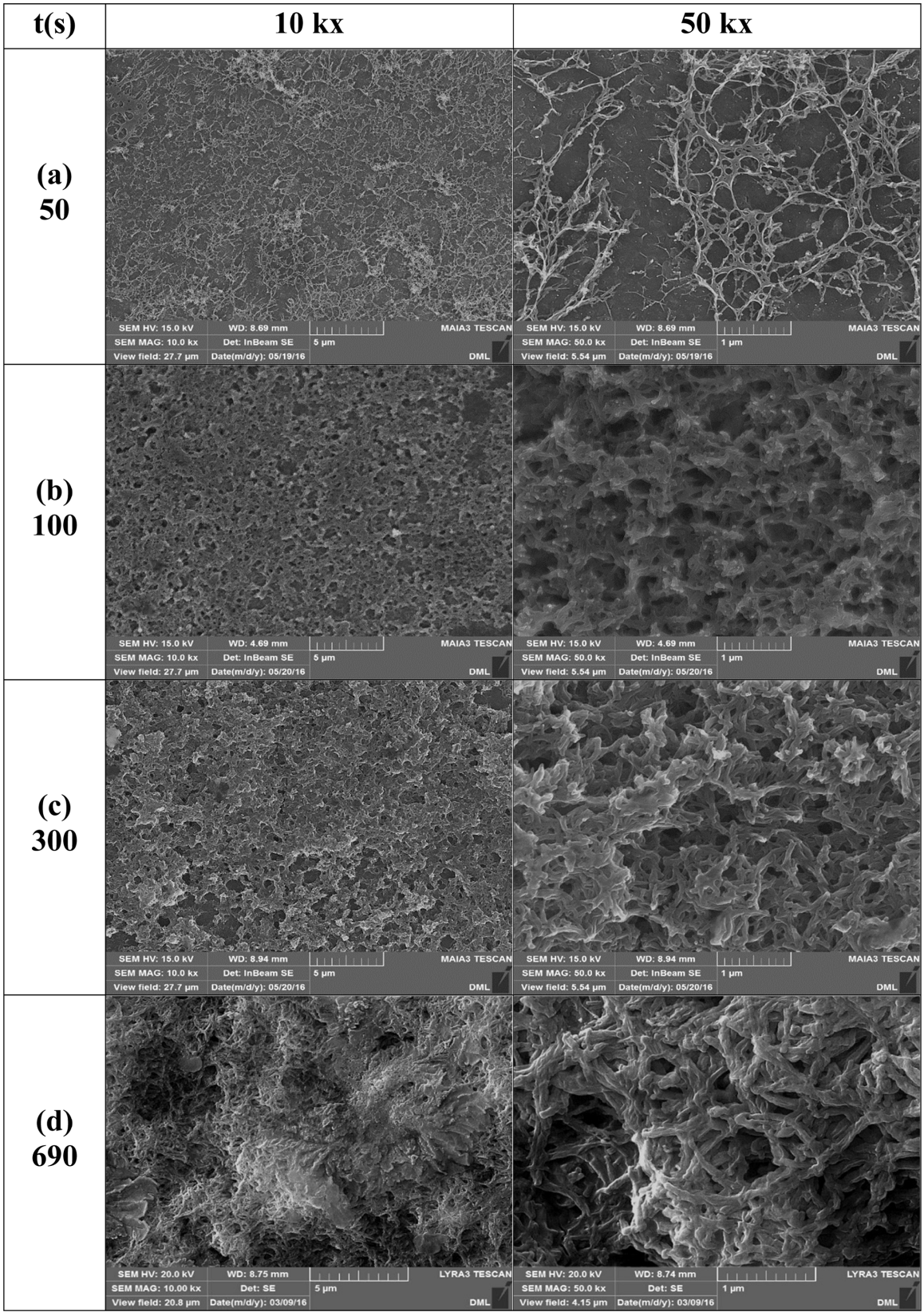

Figure 2. SEM images of PAni film at different deposition time (*t*): (a) 50 s; (b) 100 s; (c) 300 s; (d) 690 s (10 kx and 50 kx).

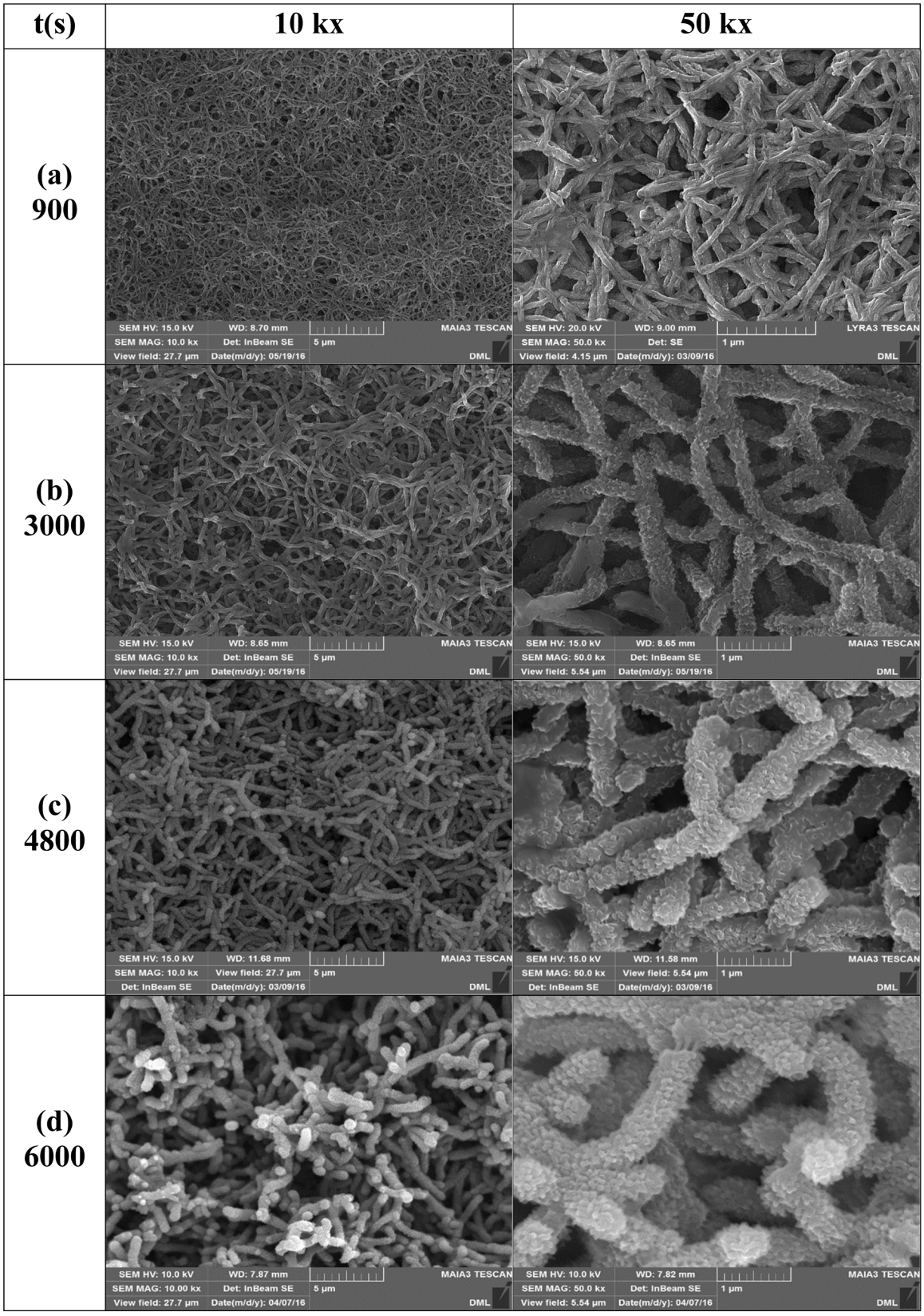

Figure 3. SEM images of PAni film at different deposition time (*t*): (a) 900 s; (b) 3000 s; (c) 4800 s; (d) 6000 s (10 kx and 50 kx).

cations by monomer oxidation at the anode. After the primary radical cations were formed, further formation of the aniline dimers occurred through deprotonation and rearomatization.[13,14] The curve shows that the polymerization was initiated as soon as the experiment started. In the R-1 (t=0~300 s), the potential increases steeply and reaches the maximum (2.67 V), which is related to the end of dimer and oligomer formation as well as the formation of a polymer layer on the bare ITO surface.[15] Once the polymer layer formed, further polymerization took place on the modified electrode and proceeded faster than on the bare ITO.[14,16] In the R-2 (t=300~900 s), the potential gradually decreases from 2.67 to 0.77 V. Since the potential required for the oxidation of the already formed polymer is low, the decreased potential was related to the polymerization of the layer already formed on the ITO.[3,14,16] In the R-3 (t=900~6000 s), the stationary potential (0.7 V) is maintained for the remaining deposition time. Since the degradation potential is close to the polymerization potential, this stationary potential indicates that polymerization and degradation compete with each other and occur simultaneously.[15,17]

SEM studies were performed at magnifications of 10 kx and 50 kx to observe the morphological changes related to the growth process of PAni. SEM images of Figure 2(a) (t=50 s) show that the polymerization started after nucleation in a short time of fewer than 50 s. SEM images are consistent with a sudden increase in potential during the first few seconds in the CP curve, as shown in the inset of Figure 1. In the R-1, the predominant horizontal growth occurs in combination with the vertical growth to form a lateral 2-D layer containing vertical polymer nodules, as shown in Figure 2(a)~(c).[10] It can be clearly seen that the whole surface of ITO is covered with the compact 2-D layer at t=300 s. In the R-2, due to the decreased contribution of 2-D growth, the polymers with a fine fibrous structure form a second layer. This second layer completely covers the first layer deposited on ITO, as shown in Figure 2(d) (t=690 s). Thus, the growth process of the second layer is not the same as the growth process of the first layer, and its morphology differs significantly from that of the first layer. In the R-3, only 1-D vertical growth occurs, and further growth results in a fibrous structure with thicker and larger diameters despite the competition between polymerization and degradation. As shown in Figure 3, the average diameter increased from ~50 nm (t=900 s) to ~350 nm (t=6000 s). It is known that several intermediates such as dimers and short chain oligomers, including soluble products such as benzoquinone and/or *p*-aminophenol, are formed during the degradation process of PAni, and these intermediates could be trapped within the film.[18,19] Due to the greatly increased degradation, large aggregates are formed and the film surface becomes coarse, as seen in Figure 3(c) (t=4800 s) and 3(d) (t=6000 s).[18] These results show that the morphological changes are related to the galvanostatic growth process proposed by the CP curve.

Figure 4 shows the temporal evolution of FTIR spectra of PAni films. FTIR spectra of electrodeposited PAni have already been published in our previous studies.[11,18] The spectrum shown in the Figure 4 exhibits the following characteristic IR bands: ~1550, ~1500, ~1270, ~1250 and ~1150 cm^{-1}. The bands at ~1550 and ~1500 cm^{-1} indicate the signature of the PAni backbone due to the stretching vibrations of the protonated quinoid (N=Q=N) ring and the benzenoid (N-B-N) rings.[20] The band at ~1270 cm^{-1} can be assigned to the π-electron delocalization induced in the polymer through protonation or C-N-C stretching vibration, while the band at ~1250 cm^{-1} is due to the $C-N^{+}$ stretching vibration in the polaron structure.[21,22] The band at ~1150 cm^{-1} is assigned to an aromatic C-H bending vibration in the plane for the 1,4-disubstituted aromatic ring, which is formed during protonation.[21] At low frequencies (<1100 cm^{-1}), the bands are related to aromatic ring deformations together with selected C-H out-of-plane vibrations.[23] The degree of oxidation (DO) of PAni can be determined by the relative intensity ratio of the band corresponding to the quinoid to benzenoid ring vibrations.[21] The relative intensity ratio ($I_{\sim1550}/I_{\sim1500}$) values for 300s, 690s, 900s, 3000s, 4800s, and 6000s are 0.80, 0.89, 0.90, 0.93, 0.95, and 0.96, respectively. A significant change was observed between the ratio for 300s (0.80) and that for 690s (0.89), suggesting a significant increase of DO in PAni molecular chains after the deposition time of 300 s. The ratio for 6000s is 0.96, which is close to 1. It bears a dark green color, further indicating that the

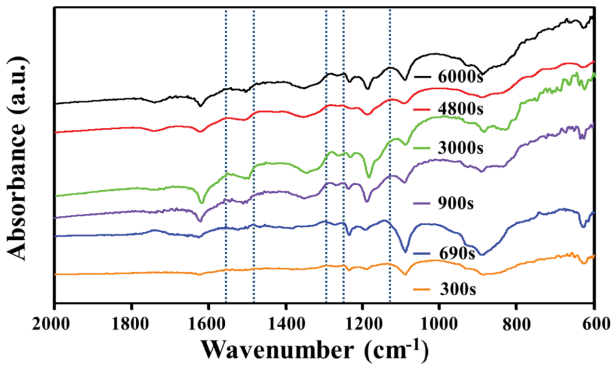

Figure 4. FTIR spectra of PAni films at different deposition times.

formation of PAni is in its doped emeraldine oxidation state.[21,22,24]

Figure 5 shows the temporal evolution of UV-Vis spectra of PAni in DMSO. PAni-EB shows two characteristic bands. The band at ~320 nm is related to the π-π* transition of the benzenoid rings. The band at ~630 nm is related to the *n*-π* transition in the quinoid rings. Through protonic acid doping of PAni-EB, imine sites are protonated to the bipolaron (dication). The bipolaron then undergoes a further rearrangement to form the delocalized polaron lattice, which is a polysemiquinone radical cation.[25] Doping of PAni-EB suppressed the band at ~630 nm, since this absorption is related to transitions in the quinoid rings, which are no longer present in the ES form, as they are converted into polysemiquinone cation radicals.[26] The resulting PAni-ES shows three characteristic bands. The band at ~300 nm is related to the π-π* transition of the benzenoid ring, whereas the band at ~450 nm is related to the polaron -π* transition; and the band at ~850 nm is related to the π- polaron transition.[25] As the bands at ~450 and ~850 nm are related to doping level and polaron formation, the doping level can roughly be estimated from the relative intensity ratio of bands at ~850 nm and ~300 nm.[27] The relative intensity ratio ($A_{\sim 850}$/$A_{\sim 300}$) for 300s, 690s, 900s, 3000s, 4800s, and 6000s are 0.12, 0.33, 0.38, 0.60, 0.97, and 0.98, respectively. Therefore, the doping level increase as deposition time increases, which can be related to DO. At the same time, as the film becomes thicker, the diffusion of counter-ions into the film becomes easier and thus the doping level increases.[28]

Electrical conductivity and sheet resistance were measured using the four-point probe technique. This technique is useful for eliminating the influence of contact resistance at the current-carrying electrodes on the measured resistance.[29] As the deposition time increases, the lower part of the film on the ITO surface becomes thicker than the upper part because gravity becomes progressively more important. Therefore, measurements were taken from multiple films. On each film, measurements were taken at five different locations, and the average of the measured values was taken. The results are presented in Table 1. In the case of the 50s, the film was too thin, so the reliability of the thickness measurement was poor and the conductivity could not be measured. As mentioned above, it is the doping process that introduces the charge carriers (polarons and bipolarons) into the polymer and renders it conductive.[2] The measured conductivity, σ, depends on both the concentration, *n*, of charge carriers and their mobility, μ. This relationship is given by $\sigma = e\, n\, \mu$, in which *e* is the elementary

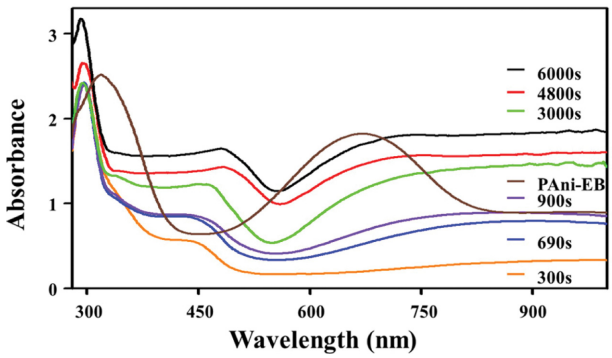

Figure 5. UV-Vis spectra of PAni at different deposition times.

Table 1. Conductivity and Sheet Resistance of PAni Films at Different Times

Film	Conductivity (S/cm)	Sheet resistance (ohm/sq.)
PAni-EB	5.00×10^{-4}	2.00×10^{5}
50s	-	7.38×10^{4}
100s	1.24×10^{-3}	7.35×10^{4}
300s	4.66×10^{-3}	7.15×10^{4}
690s	9.80×10^{-1}	3.41×10^{2}
900s	1.15	1.59×10^{2}
3000s	2.46	2.72×10^{1}
4800s	2.84	1.85×10^{1}
6000s	2.29	2.73×10^{1}

charge. In doped materials, it is not simple to distinguish whether an increase in conductivity is caused by an enhancement in the mobility of charge carriers or by an increase in the number of available mobile charge carriers.[30] Nevertheless, the doping level gradually increased and the conductivity increased (from 1.24×10^{-3} to 2.84 S/cm) while the sheet resistance decreased (from 7.35×10^{4} to 1.85×10 ohm/sq.) as the deposition time increased from 50 to 4800 s. The conductivity of 690s was markedly enhanced compared to that of 300s, which is caused by a significant improvement in charge carrier mobility as a result of the dominant 1-D vertical growth process. Despite a very high doping level, 6000s exhibits a lower conductivity (higher sheet resistance) than 4800s. This is related to the morphological changes induced by the degradation process, which shortens the polymer chains, leaving a more resistive skeleton in the polymer.[31] Figure 3(d) shows good agreement with the aggregation-induced structural disorder, which decreases the charge carrier mobility. Hence, we propose that the morphological changes that occur during the

growth process of PAni constitute an important factor influencing the increased conductivity and decreased sheet resistance.

Conclusions

This study provides evidence that the morphological change observed by SEM analysis agree with the growth process proposed from the CP curve. PAni film produced a range of very different morphologies, DO, doping levels, and sheet resistance (conductivity), depending upon the deposition time. The CP curve shows that there are three distinct regions related to the different growth process. The films electrodeposited at different deposition times exhibit different surface morphologies. A long deposition time (t=6000 s) leads to the formation of a thick film with a fibrous and aggregation-induced disordered structure due to the enhanced degradation process. Deposition time plays an important role in the formation of PAni film with different microstructures, and thus influences the charge carrier mobility. The information obtained concomitantly with the electrodeposition at a controlled potential constitutes a very useful tool for predicting working conditions aimed at controlling the film morphology.

Acknowledgement: This study is partially supported by 'SaJeDongHang' program at the center for teaching and learning of the University of Suwon.

References

1. D. N. Nguyen and H. Yoon, *Polymers*, **8**, 118 (2016).
2. R. Balint, N. J. Cassidy, and S. H. Cartmell, *Acta Biomater.*, **10**, 2341 (2014).
3. M. Gvozdenović, B. Jugović, J. Stevanović, and B. Grgur, *Hem. Ind.*, **68**, 673 (2014).
4. H. Zhang, J. Wang, Z. Zhou, Z. Wang, F. Zhang, and S. Wang, *Macromol. Rapid Commun.*, **29**, 68 (2008).
5. Y. J. Chiou, M. Y. Chung, H. M. Lin, H. Y. Liu, A. Borodzinski, L. Stobinski, C. K. Lin, and K. R. Kupiec, *J. Mat. Sci. Eng.*, **A7**, 1 (2017).
6. A. H. Le Goff and M. C. Bernard, *Synth. Met.*, **60**, 115 (1993).
7. H. Zhang, J. Wang, Z. Wang, F. Zhang, and S. Wang, *Synth. Met.*, **159**, 277 (2009).
8. M. Romero, M. A. del Valle, R. del Rio, F. R. Diaz, F. Armijo, and E. A. Dalchiele, *J. Electrochem. Soc.*, **160**, G125 (2013).
9. M. Yusairie, I. Ruhani, and F. Z. Muhammad, *IEEE Symp.*, **2012**, 1301 (2012).
10. N. T. Kemp, J. W. Cochrane, and R. Newbury, *Synth. Met.*, **159**, 435 (2009).
11. E. Kim and J.-H. Kim, *Bull. Korean Chem. Soc.*, **38**, 850 (2017).
12. E. Kim and M. Choi, *Polymer*, **40**, 728 (2016).
13. L. Arsov, W. Plieth, and G. Kossmehl, *J. Solid State Electrochem.*, **2**, 355 (1998).
14. M. M. Gvozdenović, B. Z. Jugović, J. S. Stevanović, B. Grgur, T. Lj. Trišović, and Z. S. Jugović, *Synth. Met.*, **161**, 1313 (2011).
15. S. Frangini and N. de Cristofaro, *Corros. Sci.*, **18**, 2769 (2003).
16. T. F. Otero and S. Beaumont, *Sensor Actuat. B-Chem.*, **253**, 958 (2017).
17. K. Aoki and S. Tano, *Electrochim. Acta*, **50**, 1491 (2005).
18. S. J. Choi and S. M. Park, *J. Electrochem. Soc.*, **149**, 26 (2002).
19. S. K. Mondal, K. R. Prasad, and N. Munichandraiah, *Synth. Met.*, **148**, 275 (2005).
20. G. R. Li, Z. P. Feng, J. H. Zhong, Z. L. Wang, and Y. X. Tong, *Macromolecules*, **43**, 2178 (2010).
22. E. C. Gomes and M. A. S. Oliveira, *Am. J. Polym. Sci.*, **2**, 5 (2012).
23. M. I. Boyer, S. Quillard, E. Rebourt, G. Louarn, J. P. Buisson, A. Monkman, and S. Lefrant, *J. Phys. Chem. B*, **102**, 7382 (1998).
24. X. Du, Y. Xu, L. Xiong, Y. Bai, J. Zhu, and S. Mao, *J. Appl. Polym. Sci.*, **131**, 40827 (2014).
25. K. M. Molapo, P. M. Ndangili, R. F. Ajayi, G. Mbambisa, S. M. Mailu, N. Njomo, M. Masikini, P. Baker, and E. I. Iwuoha, *Int. J. Electrochem. Sci.*, **7**, 11859 (2012).
26. A. Manzoli, C. Steffens, R. T. Paschoalin, A. A. Correa, W. F. Alves, F. L. Leite, and P. S. Herrmann, *Sensors (Basel)*, **11**, 6425 (2011).
27. T. Abdiryim, X. G. Zhang, and R. Jamal, *Mater. Chem. Phys.*, **90**, 367 (2005).
28. M. Fu, G. Shi, F. Chen, and X. Hong, *Phys. Chem. Chem. Phys.*, **4**, 2685 (2002).
29. J. A. Shetzline and S. E. Creager, *J. Electrochem. Soc.*, **161**, H917 (2014).
30. T. Stöcker, A. Köhler, and R. Moos, *J. Polym. Sci., Part B: Polym. Phys.*, **50**, 976 (2012).
31. M. J. Bleda-Martínez, C. Peng, S. Zhang, G. Z. Chen, E. Morallón, and D. Cazorla-Amorós, *J. Eletrochem. Soc.*, **155**, 1 (2008).